Macromolecular Materials and Engineering

Macromolecular Materials and Engineering Open Access

www.mame-journal.de

RESEARCH ARTICLE OPEN ACCESS

Semi-Automated Platform for Early Prenatal Coelocentesis Testing Using Electrospun Nanofiber Technology

Emanuela Muscolino[1,2] | Anna Barbara Di Stefano[3] | Santina Acuto[4] | Clelia Dispenza[1]

[1]Dipartimento Di Ingegneria, University of Palermo, Palermo, Italy | [2]Istituto Di BioFisica, Consiglio Nazionale delle Ricerche, Palermo, Italy | [3]Campus Di Ematologia Con Malattie Rare, AOOR Villa Sofia Cervello, Palermo, Italy | [4]BIOPLAST-Laboratory of BIOlogy and Regenerative Medicine-Plastic Surgery, Dipartimento Di Discipline Chirurgiche, Oncologiche e Stomatologiche, University of Palermo, Palermo, Italy

Correspondence: Emanuela Muscolino (emanuela.muscolino@unipa.it)

Received: 2 March 2026 | **Revised:** 28 April 2026 | **Accepted:** 27 May 2026

Keywords: amniocentesis | biomedical engineering | coelocentisis | chorionic villus sampling | electrospinning | microfluidics | miscarriage | nanofiber | prenatal diagnosis | prenatal diagnostics

ABSTRACT

Prenatal diagnostics play a critical role in identifying fetal disease conditions, particularly rare genetic disorders that significantly contribute to infant morbidity and mortality. Despite major advances in sequencing technologies, nearly 80% of rare disease cases remain undiagnosed. Invasive procedures such as amniocentesis and chorionic villus sampling (CVS) provide valuable genetic information but are typically performed between the 15th and 20th weeks of gestation and carry a risk of miscarriage. Non-invasive prenatal testing (NIPT) offers a safer alternative; however, it lacks the resolution required to reliably detect rare monogenic diseases. Coelocentesis, an earlier sampling technique performed between 6 and 10 weeks of gestation through transvaginal aspiration of coelomic fluid, enables access to fetal cells at a much earlier stage. Its clinical utility is limited by the low number of available fetal cells and by labor-intensive isolation methods such as micromanipulation. This study proposes a semi-automated capture device based on electrospun nanofiber mats functionalized with antibodies targeting fetal-specific surface antigens. The high surface area and structural flexibility of the nanofibers enable efficient and selective capture from low-cellularity samples. Integration with microfluidic systems may streamline processing and improve diagnostic throughput.

1 | Introduction

Prenatal diagnostics holds a central position in present-day medicine, providing expecting parents with critical information about the condition of health and development of the fetus. Prenatal diagnostics can potentially detect an array of congenital and genetic abnormalities, thus providing informed decision-making as well as preventive action for overall treatment. Prenatal diagnostics are vital for early detection of rare genetic disorders, many of which emerge during fetal development or early childhood. Though individually uncommon, rare diseases (RDs) influence the life of an estimated 263–446 million people globally [1], with about 80% of RDs having a genetic basis [2]. RDs mainly impact children, as 70%–75% present in early childhood [3] and contribute to about 35% of infant mortality. Tragically, nearly a third of affected children die before age five. They can often be identified prenatally, but despite progress in sequencing technologies, up to 80% of RD cases remain undiagnosed even with advanced tools [4].

Prenatal genetic testing is essential in the diagnostic pathway, particularly for families at known risk [5]. The testing usually involves invasive procedures like amniocentesis during the 15–20 weeks gestational period and chorionic villus sampling (CVS) during the 10–12 week gestational period, both providing a complete cytogenetic and genetic understanding. However,

these procedures have a risk of procedural miscarriage, estimated as 0.5%–1%, and are often used later in pregnancy when management options can be restricted [6].

Non-invasive prenatal testing (NIPT) based on the analysis of cell-free fetal DNA in maternal circulation has transformed screening for major aneuploidies with its high sensitivity and safety profile [7, 8]. Yet, although highly valuable for trisomy 21 and similar conditions, NIPT does not have adequate resolution for diagnosing rare single-gene diseases, a drawback that highlights the necessity of developing other early diagnostic tools [9].

An appealing addition to these well-established approaches is coelocentesis, an approach first described in the early ′90s and more recently revisited. Coelocentesis is the transvaginal aspiration of coelomic fluid from the secondary yolk sac between 6 and 10 weeks of gestation [10, 11]. The coelomic fluid aspirate contains fetal cells suitable for genetic and cytogenetic diagnosis [12]. Jouannic et al. carried out a feasibility study of coelocentesis between 8 and 9 weeks of gestation and reported successful aspiration of fetal DNA in 14 samples, with multiplex real-time PCR analyses giving amplifiable material in 71% of these, and 58% giving reliable diagnostic results [13]. Giambona et al. carried out coelocentesis at 7–9 weeks and recovered over 30 fetal cells in 25 cases out of 26 pregnancies at risk of hemoglobinopathies. Molecular analysis was feasible in all these cases, and the results were subsequently confirmed by CVS or amniocentesis [14]. Additional studies confirmed the validity of the technique for the detection of hemoglobinopathies, cystic fibrosis, and other rare monogenic disorders by 7–9 weeks of gestation [14, 15].

Coelocentesis has clear benefits: it provides an earlier diagnostic window—about 6 to 8 weeks versus 10–12 weeks for CVS—and involves a transvaginal route that does not puncture the amniotic sac or placenta, theoretically lowering the risk of the procedure [11]. Research reports over 93% diagnostic concordance between coelocentesis-derived genetic diagnoses and standard prenatal tests. However, inherent difficulties remain: fetal cells in coelomic or maternal fluids are extremely scarce, and sophisticated methods like micromanipulation or in vitro culture are needed to isolate and analyze them. The process of micromanipulation, involving manual picking of individual fetal cells under microscopic vision, is the gold standard for ensuring cell purity [16]. However, this is a labor-intensive, expensive, and highly personnel- and equipment-dependent method—factors limiting throughput and feasibility in day-to-day hospital practice [11].

The cellular density of coelomic fluid is of thousands of fetal cells per milliliter [14]. With this low concentration, the identification and isolation of a sufficient number of cells for downstream cytogenetic or molecular analyses is time-consuming. As a result, the time required to retrieve an adequate number of cells for analysis, combined with the manual and operator-dependent nature of the process, significantly constrains throughput and limits the scalability of coelocentesis-based diagnostic workflows in routine clinical practice.

Therefore, this project aims to develop the concept of a new semi-automated device to overcome these key limitations. By taking advantage of electrospun nanofiber mats functionalized with target-specific antibodies against known fetal surface antigens, the device aims to selectively trap rare fetal cells with improved efficiency.

Electrospun nanofibers have a large surface area-to-volume ratio, which is especially beneficial in biomedical applications involving effective molecular or cellular capture. Such native structural property enables multivalent interactions—concurrent binding occurrences where numerous ligands on the nanofiber surface target molecules or cells—subsequently enhancing binding strength as well as capture efficiency even in samples featuring low analyte concentrations or cellularity [17, 18]. Such qualities make electrospun fibers eminently suited for applications involving diagnostic platforms, biosensors, and enrichment devices where maximizing interaction between target and capture platform is critical [19]. Additionally, the electrospun fiber nanoscale structure can easily be modified with antibodies, aptamers, or other biomolecules, such that specificity and binding capability may be enhanced in applications involving low abundance [20].

The platform can be easily integrated into a microfluidic device, with controlled flow dynamics and real-time cell binding monitoring. The setup is expected to reduce manual variations compared to conventional micromanipulation, manual labor from specifically trained operators, and costs, making it more widely accessible. The captured fetal cells can be released and then undergo downstream conventional molecular diagnostics, like targeted PCR.

With the potential to couple early-stage sampling techniques, such as coelocentesis, with this semi-automated capture device, the research aims to simplify prenatal diagnostics. The semi-automated device is engineered with hospital scalability in consideration, since, to the best of our knowledge, there are currently no automated or semi-automated devices that exploit this diagnostic technique. By minimizing the dependence on clinician time and complex equipment, the platform has potential for wider adoption even in resource-constrained environments.

2 | Materials and Methods

2.1 | Materials

Nylon 6.6 (MW: 17 500 g/mol, ρ 1.14 g/cm3) produced by Radici Novacips SpA; Formic acid (99%–100%p.a.), aqueous solution of Polyacrylic Acid (MW: 250 000 g/mol, 35 wt. % in H2O) sodium salt of polyacrylic acid (average MW: ∼5100 g/mol, powder, 500 g), 1-ethyl-3-(3-dimethylaminopropyl)carbodiimide hydrochloride (EDC) (powder, MW: 191.70 g/mol), Sulfo-(N-hydroxysulfosuccinimide) (NHS) (powder, MW: 115. 09 g/mol), Dulbecco's phosphate-buffered saline solution (PBS) (liquid solution, 500 mL, 1X), Atto655-Biotin BioReagent (Atto655biotin) suitable for fluorescence, ≥90% (HPCE), Atto633 NHS ester BioReagent (Atto633), suitable for fluorescence, ≥90% (HPLC), SAvPhire Monomeric Streptavidin (Strept), PKH26 Red Fluorescent Cell Linker Kits for General Cell Membrane Labeling, Triton X-100, BioUltra, Molecular Biology, ∼10% in H2O, were purchased by Sigma Aldrich; eBioscienceTM Streptavidin FITC Conjugate (Strept-FITC), CD90 (Thy-1) Monoclonal Antibody Biotin eBioscience (CD90biotin), CD71 (Transferrin Receptor) Monoclonal Antibody, Biotin, eBioscience were produced by

ThermoFisher. Avidin (Avi, > 90%, Mw = 67 kDa) was kindly provided by EPS Egg Powder Specialist S.p.A. Dialysis cellulose membrane (25 mm, MWS>12000, ~60 mL/ft) produced by Sigma Aldrich. The human K562 cell line (ATCC CCL-243), originally established from a patient with chronic myelogenous leukemia in blast crisis, was purchased from the American Type Culture Collection (ATCC, Manassas, VA, USA) and maintained according to the supplier's instructions.

2.2 | Preparation of Nylon 6,6–Polyacrylic Acid Blends

A 22% wt solution of Nylon 6,6 (Ny) was prepared by dissolving the polymer in pure formic acid (FA) under constant stirring at room temperature. Separately, a 22% wt solution of polyacrylic acid (PAA) was obtained by diluting a commercial 35% wt aqueous polyacrylic acid solution with pure formic acid. The binary polymer blend NyPAA7030 was then prepared by mixing Ny and PAA solutions in a 70:30 volume ratio, maintaining the total polymer concentration at 22% wt. The final mixture was magnetically stirred at room temperature until complete homogenization.

2.3 | Electrospinning

Polymer blend solutions were electrospun using a vertical configuration with the ELECTROSPINNING MACHINE NF-103 (MECC Co., Japan). The setup included 5 mL HENKE SASS syringes (internal diameter: 12.2 mm) fitted with 22-gauge needles (0.7 mm diameter), positioned at the top of the apparatus. A rotating cylindrical collector, placed at the bottom, was covered with conductive aluminum foil.

After a preliminary optimization phase in which electrospinning parameters were systematically varied, the following conditions were selected for consistent and reproducible mat fabrication: applied voltage of 30 kV, flow rate of 0.3 mL/h, collector rotation speed of 50 rpm, needle-to-collector distance of 150 mm, and electrospinning time of 1 h and 50 min. Polymer solutions were loaded into syringes, each connected through plastic tubing and stainless steel fittings to the dispensing needle, to obtain NyPAA7030 electrospun mats (NyPAA7030_MATs).

2.4 | Scanning Electron Microscopy (SEM)

Surface morphology of NyPAA7030_MATs was analyzed using a Quanta 200 ESEM FEG field-emission scanning electron microscope. Samples were mounted on aluminum stubs (12.5 mm diameter) using adhesive carbon tape and coated with a ~10 nm layer of gold via sputter coating (EDWARDS SCANCOAT SIX, 40 s at 20 mA and 1.2 kV) to enhance conductivity.

2.5 | Thermogravimetric Analysis (TGA)

Thermal stability and compositional analysis of samples were performed using a NETZSCH STA 449 Jupiter. Approximately 10 mg of powdered sample was placed in an alumina crucible and heated from 30°C to 800°C at a rate of 10°C/min under a nitrogen atmosphere. The instrument is equipped with a high-sensitivity analytical balance and a thermocouple positioned between the sample and reference crucibles for differential temperature recording.

Thermograms display the percentage mass loss (TG%) and its derivative (DTG) as functions of temperature. Key parameters extracted include onset temperature (Tonset), maximum degradation rate temperature (Tmax), and degradation temperatures at 10% and 50% weight loss (T10% and T50%).

2.6 | Confocal Microscopy

Confocal Microscopy imaging was performed using an OLYMPUS FV1200 microscope equipped with TIRF (Total Internal Reflection Fluorescence). NyPAA7030_MATs conjugated with Streptavidin FITC, probes, and antibodies were analyzed after incubation with labeled cells. Excitation wavelengths were selected according to the fluorophores used: 488 nm (FITC), 630 nm (Atto633), 663 nm (Atto655biotin), 551 nm (PKH26).

2.7 | UV–Visible Spectroscopy

UV–visible absorption spectra were recorded using a Jasco V-670 spectrophotometer in the range of 200–800 nm, with a scan speed of 100 nm/min and a bandwidth of 1 nm. Samples were prepared by dissolving the material in a suitable solvent and transferring the solution to a quartz cuvette. All measurements were performed at room temperature and collected in triplicate to ensure reproducibility. Calibration curves were constructed by plotting absorbance values against known concentrations, following the Lambert–Beer law.

2.8 | Fluorescent Labelling of CD90biotin With Atto633 NHS Ester

The fluorescent labelling of CD90biotin antibody was performed using Atto633 NHS ester in PBS buffer (pH 7.4). Atto633 NHS ester was added to the CD90biotin solution to reach a final concentration of 0.01 mM and 0.714 μM, respectively. The reaction was carried out under light-protected conditions with continuous magnetic stirring for 4 h. After completion, the resulting conjugate was purified via dialysis using a 14 kDa cut-off membrane.

2.9 | Protein Functionalization of Electrospun Mats

Proteins were covalently conjugated to NyPAA7030_MATs (7 × 7 mm) through EDC/sulfo-NHS chemistry. In each case, carboxyl groups on the mat surface were first activated by incubation for 30 min in a PBS solution containing EDC (2.25 mM) and sulfo-NHS (4.5 mM). Proteins, such as Strept-FITC (final concentration 0.76 μM), Strept (final concentration 0.76 μM), or Avidin (final concentration 0.70 μM), previously solubilized in the same buffer, were then added directly to the activated mats. Reactions were carried out in a final volume of 0.18 mL and allowed to proceed for 6 h at 25°C under gentle

stirring. After conjugation, the systems were transferred to vials containing 3 mL of filtered PBS and subjected to a five-day washing regime, with two buffer changes per day.

2.10 | Incubation With Atto655-Biotin

NyPAA7030_MATs (7 × 7 mm) functionalized with Strept-FITC were incubated with Atto655biotin (final concentration 3.46 μM) in PBS at room temperature. The film was placed in an Eppendorf tube with the biotinylated probe, resulting in a total reaction volume of 0.12 mL. A control film of equivalent dimensions, without protein, was subjected to the same incubation conditions.

2.11 | Isolation, Culture Expansion, and Phenotypic Analysis of MSCs and WBCs

Wharton's jelly–derived mesenchymal stromal cells (MSCs) were isolated from human umbilical cords ($n = 19$) obtained after full-term caesarean deliveries with written informed consent, in accordance with the Declaration of Helsinki and with approval from the local Ethics Committee (Azienda Ospedaliera Ospedali Riuniti Villa Sofia-Cervello; approval no. 331, 08/11/2016). Umbilical cords were processed within 12 h of delivery, and MSCs were isolated by tissue explant culture as previously described [21].

Cells were cryopreserved in 90% FBS and 10% DMSO and stored in liquid nitrogen until use. Cell viability was assessed by Trypan Blue exclusion, and population doubling time was calculated using standard formulas. Mesenchymal identity was confirmed by flow cytometry based on positive expression of CD73, CD90, and CD105 and absence of CD31, CD34, CD45, and HLA-DR.

Peripheral blood lymphocytes (WBCs) were isolated from anticoagulated whole blood by density-based centrifugation. The buffy coat layer containing leukocytes was collected after centrifugation, and residual red blood cells were removed by erythrocyte lysis before experimental use.

2.12 | Preparation of Mesenchymal Stem Cell Suspension

The mesenchymal stem cell (MSC) suspension was prepared using cells incubated in their standard culture medium. To detach the MSCs, which readily adhere to culture plates, a 2.5 mL solution of proteolytic enzymes was added for 3 min following a PBS wash. The resulting suspension was then diluted with PBS to a final volume of 1.5 mL. Cell concentration was estimated using a Burker counting chamber. After centrifugation, the pellet was resuspended in PBS at a volume suitable for subsequent cell adhesion assays.

2.13 | Staining of Cell Suspensions

The mesenchymal stem cells (MSCs) were permeabilized using 0.1% Triton X-100 and stained with PKH26-red for 15 min at RT to label the cell membranes.

2.14 | Antibody Incubation

The systems were incubated with 2.5 μL of CD90biotin antibody diluted in 150 μL of PBS for 2 h at 37°C under constant agitation. Following incubation, the systems were thoroughly washed with PBS to remove unbound antibody.

2.15 | Cell Capture Assay

Cell capture assays were performed by incubating 250 000 MSCs, 125 000 MSCs, or 1000 MSCs on each antibody-conjugated system in 150 μL of PBS buffer at 37°C for 40 min under constant agitation. As a control, cells were also incubated on non-functionalized systems (films without conjugated proteins or antibodies) to perform negative tests. After incubation, all systems were thoroughly washed with PBS and subsequently fixed using 10% (w/v) formalin for 10 min. This fixation step preserved cellular morphology and maintained sample hydration for compatibility with downstream analyses with SEM or confocal analysis.

3 | Results and Discussion

This study was carried out in a series of stages aimed at developing functional electrospun nanofibrous mats capable of efficient cell capture. The first objective was to identify a suitable binary polymeric blend of Nylon 6,6 and polyacrylic acid (PAA) that could form a stable solution appropriate for electrospinning. Following the optimization of the blend composition, key electrospinning parameters were investigated to ensure the reproducibility and integrity of the resulting nanofibers. Subsequent efforts focused on the detailed morphological and physical characterization of the electrospun mats, which was critical in assessing their suitability for downstream functionalization. Finally, the optimized mats were subjected to chemical conjugation and evaluated for their performance in targeted cell capture applications.

3.1 | Optimization of Polymeric Blend Composition and Electrospinning

Different approaches were explored to prepare a binary polymeric blend of Nylon 6,6 and polyacrylic acid. An initial attempt using a 50:50 ratio resulted in rapid gelation of the mixture within 24 h, making it unsuitable for electrospinning. A second strategy involved dissolving Nylon 6,6 directly into PAA solution, followed by the addition of formic acid. However, this method led to only partial solubilization of Ny.

The only formulation that yielded a stable, electrospinnable blend was achieved by simultaneously and progressively adding small droplets of a Ny solution in pure formic acid (22%w) and a PAA aqueous solution (22%w) into a beaker under constant magnetic stirring to obtain a 70:30 volume ratio between the two solutions (NyPAA7030). The viscosity and homogeneity of the resulting solution were highly dependent on the addition rate. Rapid addition induced the formation of flocculates, compromising the uniformity and usability of the mixture for electrospinning.

After the appropriate conditions to produce the two polymer blends were found, electrospinning was attempted. Several

TABLE 1 | Optimized electrospinning parameters used for the fabrication of NyPAA7030_MATs. These conditions were selected to ensure consistent fiber morphology, reproducibility, and efficient mat formation.

Parameter	Value
High voltage	30 kV
Flow rate	0.3 mL/h
Collector rotation speed	50 rpm
Needle traverse speed	30 mm/s
Needle-to-collector distance	150 mm
Electrospinning duration	1 h 50 min

parameters were fine-tuned to produce the most consistent and reproducible nanofiber mats. The optimized parameters used to produce the most structurally consistent mats are summarized in Table 1. Electrospun mats were optimized based on morphological quality, structural integrity, and processing efficiency. Initial attempts to remove nanofibers from plain aluminum foils often resulted in fiber damage due to strong adhesion. To overcome this, the mats were collected onto parchment film strips applied over aluminum, allowing for non-destructive separation. Given the extended electrospinning durations required to obtain adequate mat thickness, the use of dual-syringe configurations was adopted to reduce processing time.

Electrospun mats obtained from binary polymer blends were characterized for their morphological properties, including nanofiber diameter, distribution, and structural uniformity. Morphologies were assessed using SEM. Nanofiber diameters were quantified using ImageJ and the DiameterJ plugin. SEM samples were prepared by mounting mat fragments on aluminum stubs with adhesive tape and coating with a gold layer (~10 nm) via sputtering. The SEM images (Figure 1A) of the front side (outer) of NyPAA7030_MAT detached from the parchment film shows a randomly oriented nanofiber network with smooth surfaces and no apparent porosity. Diameters were broadly distributed, with most fibers in the 300–400 nm range. The histogram in Figure 1B confirms a wide size distribution with a peak in this range. As shown in Figure 1, the reverse (inner) side of the same mat displayed defects caused by the accumulation of solution droplets prior to electrospinning jet stabilization. Although these irregularities were evident at low magnification, higher-magnification imaging revealed fibers with a morphology comparable to that of the front side.

The observed fiber diameter distribution (predominantly 300–400 nm) may influence cell capture performance, as fiber size directly affects surface area, topography, and cell–material interactions. In general, smaller fiber diameters provide a higher surface-area-to-volume ratio, which can enhance antibody immobilization density and increase the probability of cell–capture [22]. Conversely, larger fibers may contribute to improved mechanical stability giving the device more structural integrity. The relatively broad diameter distribution observed in this study may therefore offer a balance between these effects, combining high surface area with structural robustness.

TGA was employed to investigate the thermal stability and composition of polymer mats composed of Ny and PAA. The thermograms of electrospun mats and solvent-cast films were compared with those of the individual polymers to evaluate their degradation behavior and mutual interactions.

The solvent-cast Ny exhibited a single major degradation event, with a total mass loss of approximately 95% and a T_{onset} of 430°C (Figure 2A). A small mass loss (~4%) between 30°C and 100°C was attributed to moisture release. The PAA film showed a three-step degradation profile, with mass losses of 14% at 135°C, 23% at 287°C, and 45% at 444°C, resulting in a total mass loss of 87% and a carbonaceous residue.

The binary blend (NyPAA7030) displayed a degradation profile reflecting contributions from both polymers, but with notable shifts. In particular, the degradation onset of PAA-related transitions occurred at higher temperatures, indicating intermolecular interactions that enhance thermal stability. The NyPAA7030_MAT exhibited similar behavior, with major weight losses observed at 224°C and 437°C, and an overall mass loss of 89%. These results suggest that blending influences the thermal degradation pathway, likely due to hydrogen bonding or ionic interactions between the two polymer chains, which hinder their early decomposition [23].

Microraman spectroscopy was employed to investigate the chemical composition of both electrospun NyPAA7030_MAT and cast films derived from the individual polymer components (Figure 2B). The spectrum of the Ny component shows the characteristic bands of Nylon 6,6 reported in the literature [24], including the C–H bending and stretching modes at ~1440 and ~3300 cm^{-1}, the carbonyl band at ~1640 cm^{-1}, and the N–H-related peaks at ~2900 and ~1200 cm^{-1}. The Raman spectrum of the NyPAA7030_MAT displayed similar dominant features attributable to Nylon 6,6, which is expected given its higher proportion in the blend and new spectral contributions from PAA. In particular, the peak at 1751 cm^{-1} is attributed to the carboxylic acid groups of PAA. Additionally, a slight shift in the carbonyl band (~1648 cm^{-1}) may reflect hydrogen bonding or intermolecular interactions between the two polymers [25].

These results confirm the successful incorporation of PAA into the nanofibrous matrix and further support the postulated attractive interactions between Ny and PAA chains. It is worth highlighting that solvent casting of the binary blend leads to a macroscopically phase-separated system. In solution, in their respective solvents, both polymers adopt a random coil conformation that is expanded due to electrostatic repulsion among fixed electric charges along the chain: in unbuffered PAA aqueous solutions, carboxyl groups are partially deprotonated, while formic acid can protonate the N–H groups of the amide of Ny, breaking interchain hydrogen bonds. The strong electrostatic field and elongational flow of the electrospinning process stretch further the chains of both polymers along the fiber axis, leading to more extended and oriented conformations, favoring their mutual interactions, both electrostatic and hydrogen bonding.

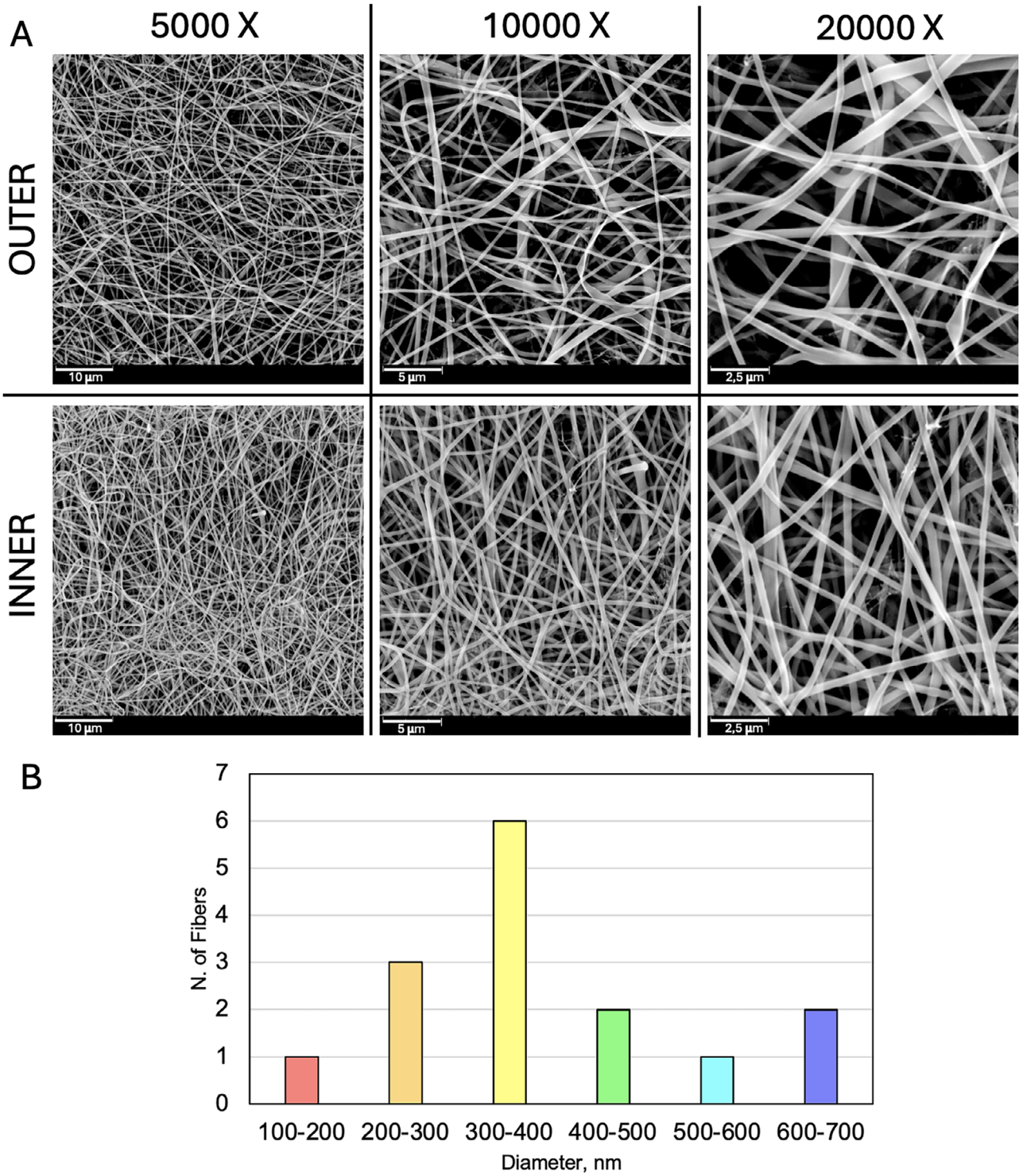

FIGURE 1 | (A) Scanning electron microscopy (SEM) images of the NyPAA7030_MATs showing the front (outer) and back (inner) surfaces at magnifications of 5000 X, 10000 X, and 20000 X. (B) Histogram of fiber diameters distribution.

3.2 | Surface Conjugation and Functionalization

The functionalization of nanofibrous mats is a critical step in enabling their application for diagnostic purposes. To achieve specific and stable molecular attachment on the surface of electrospun mats, a bioconjugation strategy utilizing the high-affinity interaction between biotin and streptavidin was employed. This approach offers several advantages, including strong non-covalent binding, spatial specificity, and compatibility with a variety of biotinylated probes and antibodies [26].

To verify effective bioconjugation, the validation began with a model conjugation system designed to assess the fundamental biotin-streptavidin interaction on the mats. NyPAA7030_MATs functionalized with Strept-FITC were then incubated with Atto655biotin, a small-molecule fluorescent probe (Figure 3A).

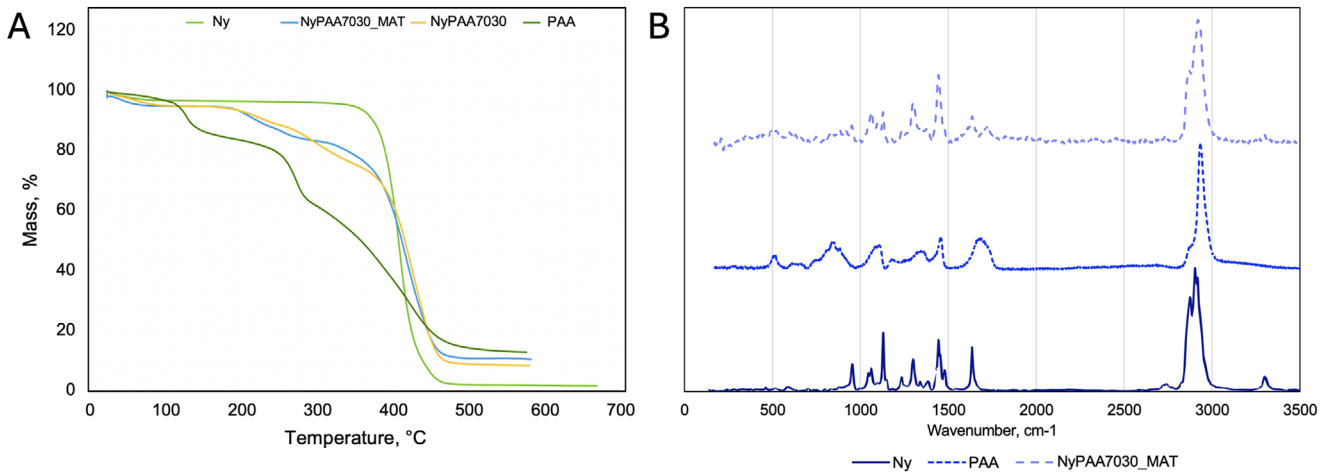

FIGURE 2 | (A) Thermogravimetric analysis (TGA) curves of solvent-cast Ny, solvent-cast PAA, NyPAA7030 blend film, and electrospun NyPAA7030_MAT; (B) Micro-Raman spectra of Ny, PAA, and NyPAA7030_MAT.

The successful functionalization of electrospun nanofibrous mats was evaluated using confocal microscopy, which offers depth-resolved imaging. Due to the three-dimensional architecture of the electrospun mats, quantitative fluorescence analysis was not performed; however, confocal z-stack imaging provides spatially resolved evidence of uniform functionalization throughout the mat. The resulting images, shown in Figure 3B, demonstrated strong and uniform green fluorescence from streptavidin, alongside a clearly overlapping red signal from the Atto655biotin. The first two rows display the green fluorescence signal corresponding to streptavidin-FITC acquired as a z-stack, revealing its distribution throughout several micrometers of the mat thickness. The third and fourth rows show the red fluorescence signal from Atto655-biotin, also acquired as a z-stack, indicating that the biotinylated probe is able to penetrate and bind to streptavidin throughout the fibrous network rather than being limited to the surface.

The merged images (bottom rows) demonstrate a high degree of spatial colocalization between the green and red signals across the imaged depth, confirming that the biotin–streptavidin interaction occurs throughout the three-dimensional structure of the mat. This result supports effective and uniform functionalization of the electrospun scaffold.

Following this validation, a more complex bioconjugation system was implemented to demonstrate the platform's capability for anchoring biologically relevant molecules. To achieve dual bioconjugation, CD90biotin had first been successfully labeled with the red fluorescent dye Atto633. Spectrophotometric analysis confirmed the successful conjugation of the CD90biotin antibody with the Atto633NHS-ester fluorescent probe. After dialysis, excitation at λ_{exc} = 633 nm yielded an absorbance of 0.089, corresponding to a probe concentration of 0.0007 mM and a conjugation degree of 0.92 mol of Atto633 per mol of CD90biotin. Hence, the resulting conjugation efficiency was 92%, validating the high yield of the labeling procedure. Subsequently, the mats functionalized with streptavidin-FITC were incubated with the labeled CD90biotin (Figure 4A). This setup enabled simultaneous visualization of both the streptavidin anchoring platform and the targeted antibody.

Confocal imaging (Figure 4B) revealed a uniform green fluorescence signal from the FITC-labeled streptavidin throughout the mat, observable across multiple focal planes. Again, this indicated that streptavidin had been successfully and evenly distributed across the fibrous network, without clustering or local voids. The red fluorescence signal (in magenta) from the Atto633-labeled CD90biotin was also consistently observed across the same depth profiles, further suggesting efficient and homogeneous antibody immobilization. When the green and red channels were merged, extensive colocalization was evident, supporting the conclusion that the antibody had specifically and stably bound to the streptavidin layer. These results collectively confirm the effectiveness of the bioconjugation strategy, both in terms of chemical specificity and spatial consistency.

Together, these findings provide clear evidence that the surface of the electrospun mats can be reproducibly and uniformly functionalized using streptavidin-based coupling strategies. The consistent spatial distribution of both protein and probe species across the scaffold confirms that the fiber surfaces are accessible and that the conjugation reactions proceed efficiently throughout the material volume. This is a critical requirement for downstream applications such as targeted cell capture.

3.3 | Cell Capture Assays

Primary coelomic fluid samples were not employed for assay development due to their extremely limited availability and their prioritization for clinical diagnostic use. Model cell lines (K562) and MSCs were used as control systems to evaluate capture efficiency and antibody specificity, given the limited accessibility of primary coelomic fluid samples. While these models cannot fully reproduce the complexity of clinical samples, they provide a necessary first step in the development of the platform.

As a proof of concept for antibody selectivity, a set of experiments was performed using mats functionalised with anti-CD71 antibodies. Positive controls were conducted with the K562 cell line (a cell line expressing the same CD71 as fetal cells), and negative controls included MSCs and white blood cells (WBCs).

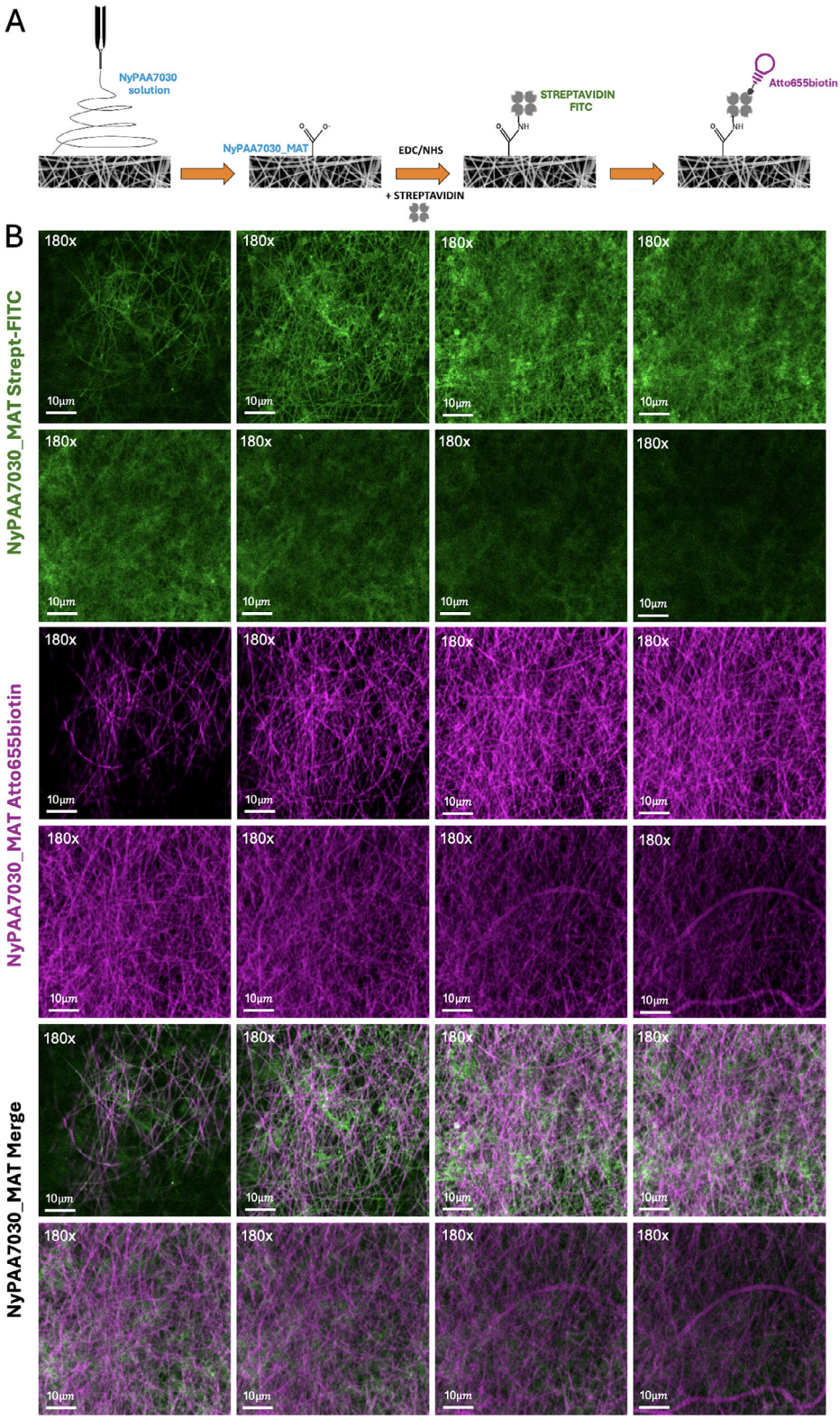

FIGURE 3 | (A) Schematic illustration of electrospinning of the NyPAA7030 solution followed by mat surface activation using EDC/sulfo-NHS chemistry for covalent conjugation of Strept-FITC, and subsequent binding of Atto655biotin. (B) Confocal microscopy images (180×) in Z-stack of NyPAA7030_MATs functionalized with Strept-FITC (green) and incubated with Atto655biotin (magenta) and corresponding merged channels at 180× magnifications.

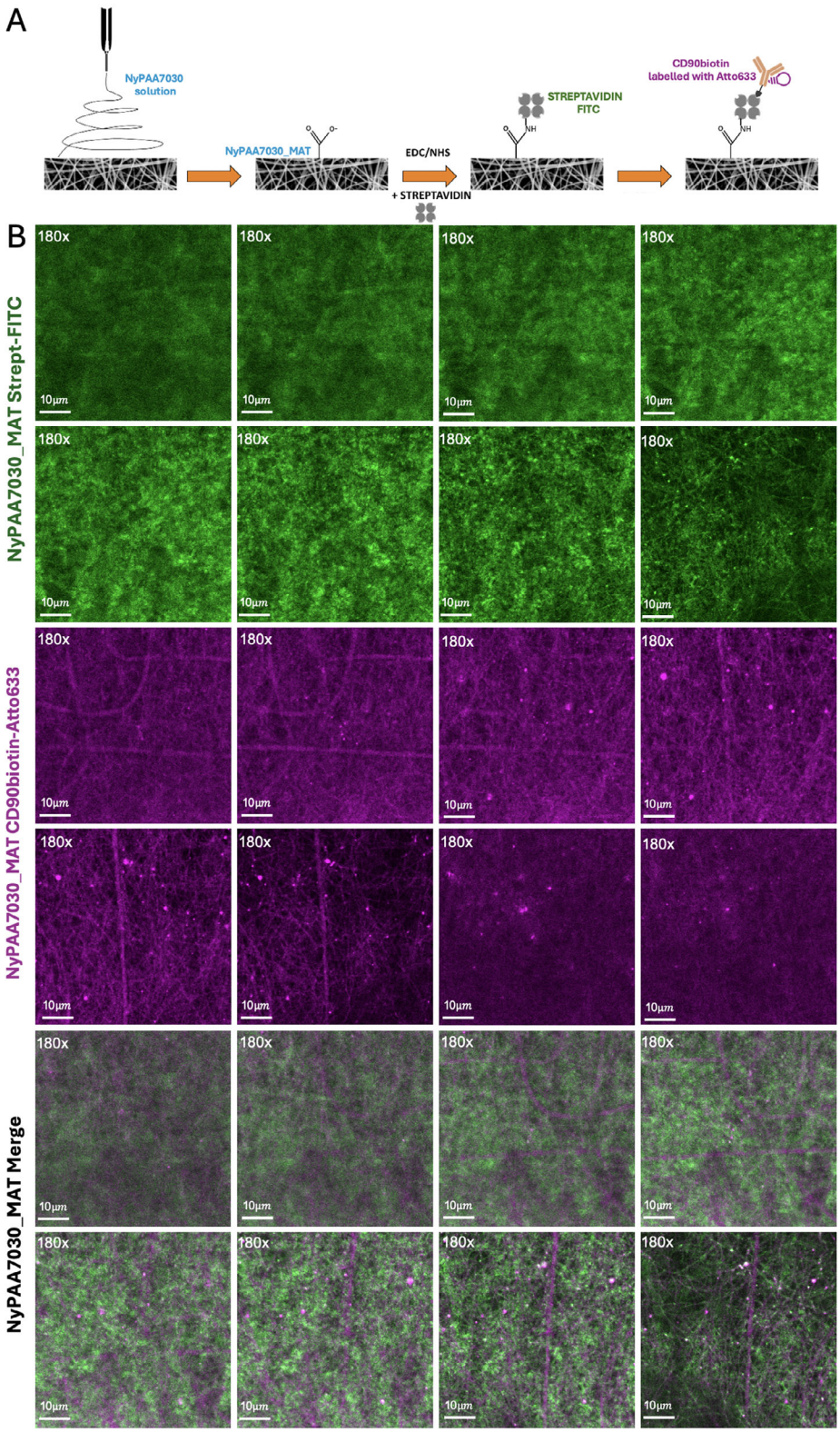

FIGURE 4 | (A) Schematic illustration of electrospinning of NyPAA7030 followed by EDC/sulfo-NHS activation, covalent immobilization of streptavidin-FITC, and subsequent binding of biotinylated anti-CD90biotin labeled with Atto633. (B) Confocal microscopy images (180×) in Z-stack of NyPAA7030_MATs functionalized with Atto633-labeled streptavidin-FITC (green), CD90biotin (magenta), and corresponding merged channels.

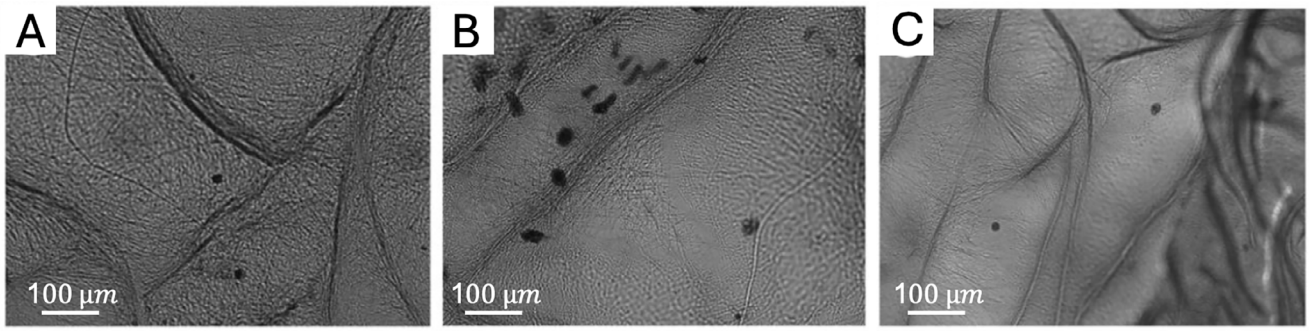

FIGURE 5 | Optical microscopy images (40×) of anti-CD71–conjugated mats under different cell exposure conditions: (A) NyPAA7030_MAT in the presence of WBCs; (B) NyPAA7030_MAT in the presence of K562 cells; and (C) NyPAA7030_MAT in the presence of MSCs.

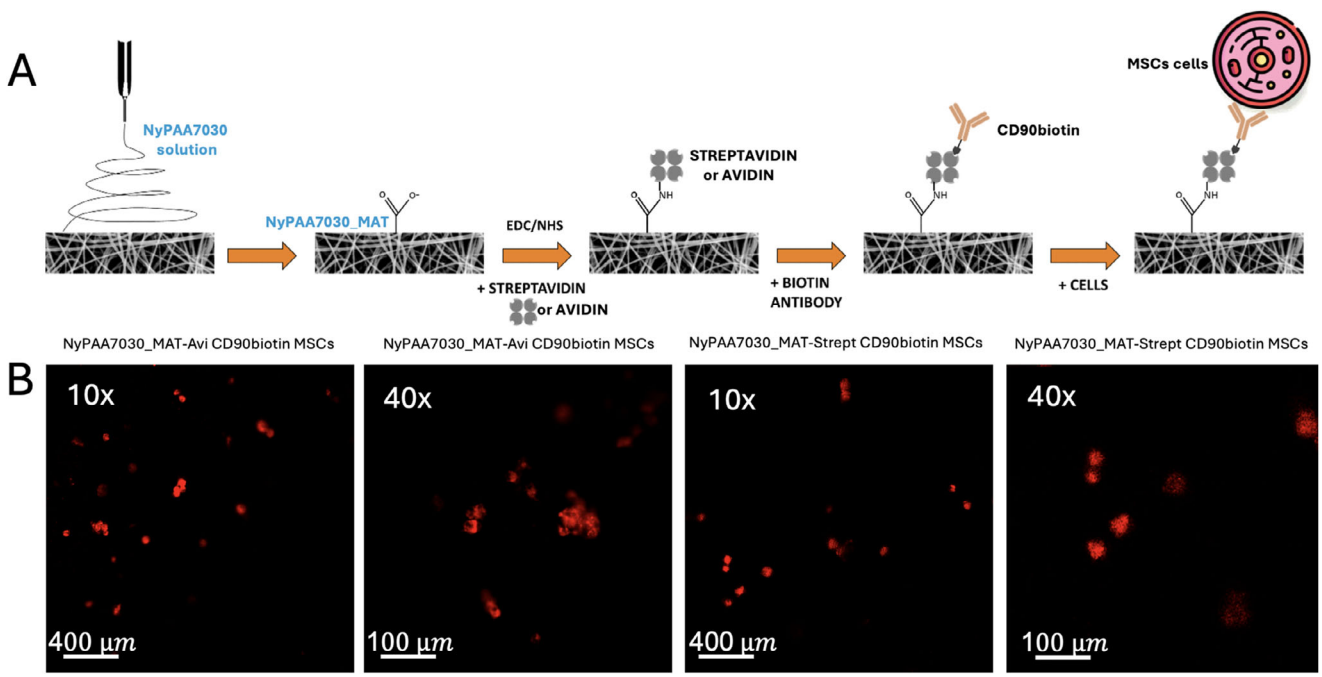

FIGURE 6 | (A) Schematic illustration of electrospinning of NyPAA7030, surface activation via EDC/NHS chemistry, immobilization of Strept or Avi, subsequent decoration of CD90biotin, and MSCs capture, (B) Confocal microscopy images of PKH-labeled MSCs adhesion on Strept- and Avi-based and CD90biotin functionalized NyPAA7030_MAT following high-density seeding (250 000 cells per substrate) at 10× and 40× magnifications.

The results confirmed the selective capture capability of the system: some FCs were observed (Figure 5B), and practically no MSCs or WBCs were retained on the surface (Figure 5A,C). These findings support the substrate potential for selective cell targeting, particularly when combined with appropriate surface chemistry and antibody functionalization.

Further cell capture assays were carried out using CD90biotin antibody and mesenchymal stem cells (MSCs, a CD90-expressing cell type) as a model target due to the major availability during the study. The designed device was constituted by the NyPAA7030_MAT conjugated to Strept and then incubated with the CD90biotin antibody for cell capture (Figure 6A). The same design was applied to a second device that used avidin (Avi) instead of streptavidin to verify if the same results could be obtained with another commercially available biotin-binding protein. To reduce spectral interference, FITC labeling was omitted for these capture assays. Capture efficiency was assessed under varying experimental conditions to evaluate the robustness and reproducibility of the systems. In the first phase, a preliminary high-density seeding of 250 000 MSCs per substrate was performed to confirm general cell adhesion across the surfaces (data shown in Figure 6). The presence of cells was observed through confocal microscopy, using PKH-labeled MSCs, which confirmed cell presence.

Following successful adhesion, the systems were challenged with lower cell concentrations (125 000 MSCs per substrate) to assess performance over time. Substrates aged at different intervals (newly prepared, 1 month old, and 3 months old) were included to evaluate the stability of functionalization over storage (Figure 7A). In all cases, no significant differences in cell capture

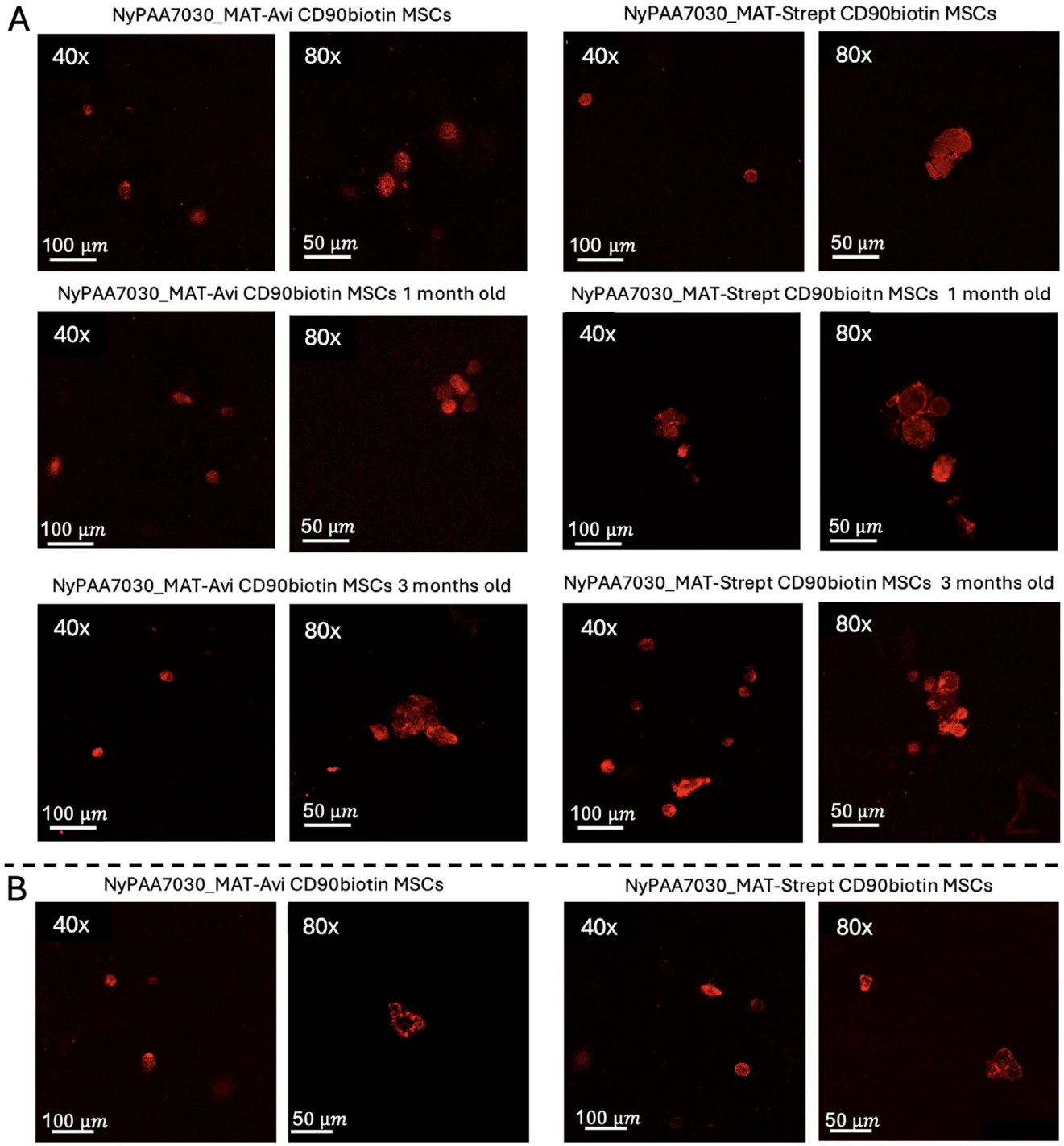

FIGURE 7 | Confocal fluorescence microscopy images at 40× and 80× magnifications of PKH-labeled MSCs (red) capture on avidin- or streptavidin-functionalized NyPAA7030_MATs decorated with CD90biotin at: (A) reduced cell density (125 000 MSCs per substrate), substrates prepared at different aging times (freshly prepared, 1 month, and 3 months); (B) very low cell density of 1000 MSCs per substrate.

were observed across timepoints or between avidin and streptavidin systems, suggesting that substrate integrity and functional binding capacity were well maintained. No significant differences between avidin and streptavidin systems were observed.

In the final and most stringent condition, a low concentration of 1000 MSCs per system was tested (Figure 7B). These conditions resemble the concentration of fetal cells in coelomic fluid harvested by coelocentesis that ranges from hundreds to thousands of cells per milliliter [14]. Even under these conditions, all systems demonstrated some degree of cell adhesion with no significant difference between avidin and streptavidin-based capture surfaces. This consistency across conditions suggests that the primary limiting factor may not be the cell number itself, but rather the number of active binding sites available or reachable on the substrate surface. The substrates provide a functional base, but device design may constrain binding efficiency at very low target concentrations.

Currently, coelocentesis-based fetal cell isolation is not supported by standardized or automated platforms and relies on manual, operator-dependent procedures performed in specialized centers. This limits direct comparison with existing automated prenatal diagnostic technologies. An indirect comparison of the proposed platform with existing prenatal diagnostic approaches can be considered across key clinical metrics. In terms of diagnostic window, coelocentesis enables access to fetal material at earlier gestational stages (approximately 7–9 weeks) compared to amniocentesis or CVS (typically ≥15 weeks) [11], potentially allowing earlier clinical decision-making. However, coelocentesis is a more technically demanding procedure and is not yet widely standardized. Regarding labor requirements, current coelocentesis workflows rely on manual micromanipulation techniques for fetal cell isolation, making them expensive, time-consuming, and difficult to scale in a clinical setting, as not many samples can be analyzed daily. The proposed platform aims to reduce operator dependency by introducing a more standardized capture interface. The proposed design would cut costs when compared with the current way coelocentesis is performed by cutting human labor and the need for expensive equipment such as the micromanipulator. It would also reduce the time for fetal cell isolation, granting faster processability of samples, allowing for a greater volume of patients.

In terms of diagnostic accuracy, fetal cells obtained from coelomic fluid are suitable for the same downstream cytogenetic and molecular analyses routinely performed on amniotic fluid samples, enabling a potentially definitive diagnostic outcome [10, 11].

When comparing with current diagnostic devices, it must be considered that this study considers fetal cells in coelomic fluid as a target. The cellular density of coelomic fluid—often reaching thousands of fetal cells per milliliter [14]—fundamentally differs from the sparse fetal-cell landscape of maternal blood (typically 1–20 fetal cells per 10 mL). This high fetal content reduces the need for complex rare-cell enrichment steps that can be used in cell-based non-invasive prenatal test (cbNIPT) workflows using blood.

Companies that are focusing on prenatal diagnostics on a clinical level, such as Vanadis [27] and Prenatalsafe [28], use cell-free fetal DNA found in the mother's bloodstream as a target. It is important to point out that currently this solution serves only as a screening device and can be used only later on in the pregnancy [29, 30]. In contrast, coelocentesis enables the retrieval of coelomic fluid at very early gestational ages (approximately 7–9 weeks) and provides access to intact fetal cells and high-molecular-weight fetal DNA, allowing direct and potentially definitive genetic analysis, comparable to an actual diagnostic tool.

Multi-stage systems such as ISET paired with Rarecells [31], ScreenCell [32] or Parsortix [33], DEPArray [34], RareCyte [35] are clinically employed to capture circulating tumor cells (CTCs). Although these companies are expanding their target to prenatal diagnostic (only at the research level at the moment), these platforms entail substantial per-sample costs, complex sample preparation, and are optimized for extremely low target frequencies.

Furthermore, when applied to coelomic fluid, the physical enrichment capabilities of these commercial systems offer limited benefit. The challenge shifts from rare-cell detection to preserving cells and minimizing processing-induced loss or damage. Under such conditions, direct immunoaffinity-based capture surfaces represent a technically and economically attractive alternative. Antibody-functionalized mats simplified workflow logistics, reduced reagent, and consumable costs. The main limitations of such approaches remain the need for robust quality control of antibody coatings, potential non-specific binding of maternal cells, and the lack of standardized release chemistries for downstream analysis.

To address this weakness, ongoing studies are exploring the possibility of expanding the effective surface area via microfluidic integration, which may enhance substrate–fluid contact and increase the likelihood of rare cell capture by exposing a greater number of active binding sites and release chemistry with cleavable linkers.

Overall, these results highlight the potential of the Ny/PAA-based platforms and lay the foundation for optimization aimed at increasing capture fidelity, especially for diagnostic applications and rare cell isolation, where sensitivity and specificity are vital.

4 | Conclusions

This study has demonstrated how the engineering of nanofibrous matrices, obtained by electrospinning a binary blend of Nylon 6,6–polyacrylic acid, can provide a functional and scalable platform for selective cell capture. The effectiveness of the surface functionalization, based on the biotin–streptavidin interaction, was demonstrated by the consistent and depth-resolved colocalization of fluorescent signals from streptavidin-FITC and biotinylated probe or labeled biotinylated antibody throughout the nanofibrous structure, indicating stable and homogeneous immobilization of bioactive molecules.

The importance of these results lies not only in the validation of a technically robust and long-lasting material but also in its versatility and adaptability to real-world applications, such as early diagnostics or the isolation of rare cells from complex biological samples. The observed performance indicates that the main limitation may lie in the lack of fluid interaction between cellular targets and binding sites. However, the systems were able to capture some cells even with a small number of cells/ml (comparable to real-life coelomic fluid), and the actual number of cells necessary for prenatal diagnostic analysis is not high. In fact, prenatal diagnosis can be carried out even with about 30 cells [14].

Therefore, the work opens concrete prospects for integrating these matrices into microfluidic systems or portable devices, with the aim of increasing efficiency and transforming them into useful tools for highly sensitive clinical applications. Future work will focus on clinical validation using primary coelomic fluid samples to assess the performance of the platform in real diagnostic settings. More generally, the results obtained confirm the potential of functionalized nanofiber-based technologies as platforms for targeted cell capture, representing a step forward in advanced diagnostic solutions.

Author Contributions

Emanuela Muscolino: conceptualization, investigation, writing – original draft, methodology, validation, visualization. **Anna Barbara Di Stefano:** investigation, methodology, visualization, validation. **Santina Acuto:** conceptualization, investigation, resources, validation, methodology, visualization. **Clelia Dispenza:** conceptualization, funding acquisition, writing – review & editing, supervision, resources, project administration.

Acknowledgements

The authors gratefully acknowledge Monica La Milia and Federica Giuliano for their valuable support in this research.

Open access publishing facilitated by Universita degli Studi di Palermo, as part of the Wiley - CRUI-CARE agreement.

Funding

Emanuela Muscolino was funded from the European Union—NextGenerationEU through the Italian Ministry of University and Research, under PNRR—M4C2-I1.3 Project PE_00000019 "HEAL ITALIA" CUP B73C22001250006. The ideas voiced are just those of the authors and do not automatically reveal those of the European Commission or the European Union. Neither the European Commission nor the European Union should be held accountable for them.

Conflicts of Interest

The authors declare no conflicts of interest.

Data Availability Statement

The data that support the findings of this study are available from the corresponding author upon reasonable request.

References

1. S. Nguengang Wakap, D. M. Lambert, and A. Olry, et al., "Estimating Cumulative Point Prevalence of Rare Diseases: Analysis of the Orphanet Database," *European Journal of Human Genetics* 28 (2020): 165–173, https://doi.org/10.1038/s41431-019-0508-0.

2. H. Gürkan and N. B. Satkın, "The Importance of Genetic Diagnosis in Rare Diseases," *Balkan Medical Journal* 42 (2025): 92–93, https://doi.org/10.4274/balkanmedj.galenos.2025.2025-270125.

3. E. Gunne, C. McGarvey, K. Hamilton, E. Treacy, D. M. Lambert, and S. A. Lynch, "A Retrospective Review of the Contribution of Rare Diseases to Paediatric Mortality in Ireland," *Orphanet Journal of Rare Diseases* 15 (2020): 311, https://doi.org/10.1186/s13023-020-01574-7.

4. S. Marwaha, J. W. Knowles, and E. A. Ashley, "A Guide for the Diagnosis of Rare and Undiagnosed Disease: Beyond the Exome," *Genome Medicine* 14 (2022): 23, https://doi.org/10.1186/s13073-022-01026-w.

5. L. S. Rosenblum, S. M. Auger, H. Zhu, et al., "Prenatal Testing for Variants in Genes Associated With Hereditary Cancer Risk," *The Journal of Molecular Diagnostics* 26 (2024): 202–212, https://doi.org/10.1016/j.jmoldx.2023.12.002.

6. L. J. Salomon, A. Sotiriadis, C. B. Wulff, A. Odibo, and R. Akolekar, "Risk of Miscarriage Following Amniocentesis or Chorionic Villus Sampling: Systematic Review of Literature and Updated Meta-Analysis," *Ultrasound in Obstetrics & Gynecology* 54 (2019): 442–451, https://doi.org/10.1002/uog.20353.

7. M. Abedalthagafi, S. Bawazeer, R. I. Fawaz, A. M. Heritage, N. M. Alajaji, and E. Faqeih, "Non-Invasive Prenatal Testing: A Revolutionary Journey in Prenatal Testing," *Frontiers in Medicine* 10 (2023): 1265090, https://doi.org/10.3389/fmed.2023.1265090.

8. S. Lee, J. H. Choi, J. H. Yun, et al., "Clinical Applications and Advancements in Noninvasive Prenatal Diagnosis," *Kosin Medical Journal* 40 (2025): 106–115, https://doi.org/10.7180/kmj.25.118.

9. M. A. Lutgendorf, K. A. Stoll, D. M. Knutzen, and L. M. Foglia, "Noninvasive Prenatal Testing: Limitations and Unanswered Questions," *Genetics in Medicine* 16 (2014): 281–285, https://doi.org/10.1038/gim.2013.126.

10. D. Aiello, A. Giambona, F. Leto, et al., "Human Coelomic Fluid Investigation: A MS-Based Analytical Approach to Prenatal Screening," *Scientific Reports* 8 (2018): 10973, https://doi.org/10.1038/s41598-018-29384-9.

11. &G. Makrydimas, G. Damiani, C. Jakil, et al., "Celocentesis for Early Prenatal Diagnosis of Hemoglobinopathy," *Ultrasound in obstetrics & Gynecology: the official journal of the International Society of Ultrasound in Obstetrics and Gynecology* 56 (2020): 672–677, https://doi.org/10.1002/uog.22059.

12. J.-M. Jouannic, G. Tachdjian, J.-M. Costa, and J.-L. Bénifla, "Coelomic Fluid Analysis: The Absolute Necessity to Prove Its Fetal Origin," *Reproductive BioMedicine Online* 16 (2008): 148–151, https://doi.org/10.1016/S1472-6483(10)60568-8.

13. J.-M. Jouannic, J.-M. Costa, P. Ernault, and J.-L. Bénifla, "Very Early Prenatal Diagnosis of Genetic Diseases Based on Coelomic Fluid Analysis: A Feasibility Study," *Human Reproduction* 21 (2006): 2185–2188, https://doi.org/10.1093/humrep/del143.

14. A. Giambona, G. Makrydimas, F. Leto, et al., "Feasibility of DNA Diagnosis of Haemoglobinopathies on Coelocentesis," *British Journal of Haematology* 153 (2011): 268–272, https://doi.org/10.1111/j.1365-2141.2011.08621.x.

15. A. Giambona, M. Vinciguerra, F. Leto, et al., "Prenatal Diagnosis of Cystic Fibrosis by Celocentesis," *Genes* 15 (2024): 662, https://doi.org/10.3390/genes15060662.

16. A. Giambona, M. Vinciguerra, F. Leto, et al., "Celomic Fluid: Laboratory Workflow for Prenatal Diagnosis of Monogenic Diseases," *Molecular Diagnosis & Therapy* 26 (2022): 239–252, https://doi.org/10.1007/s40291-022-00577-3.

17. A. Greiner and J. H. Wendorff, "Electrospinning: A Fascinating Method for the Preparation of Ultrathin Fibers," *Angewandte Chemie International Edition* 46 (2007): 5670–5703, https://doi.org/10.1002/anie.200604646.

18. D. Li and Y. Xia, "Electrospinning of Nanofibers: Reinventing the Wheel?," *Advanced Materials* 16 (2004): 1151–1170, https://doi.org/10.1002/adma.200400719.

19. N. Bhardwaj and S. C. Kundu, "Electrospinning: A Fascinating Fiber Fabrication Technique," *Biotechnology Advances* 28 (2010): 325–347, https://doi.org/10.1016/j.biotechadv.2010.01.004.

20. X. Wang, B. Ding, and B. Li, "Biomimetic Electrospun Nanofibrous Structures for Tissue Engineering," *Materials Today* 16 (2013): 229–241, https://doi.org/10.1016/j.mattod.2013.06.005.

21. S. Acuto, M. Lo Iacono, E. Baiamonte, R. Lo Re, A. Maggio, and V. Cavalieri, "An Optimized Procedure for Preparation of Conditioned Medium From Wharton's Jelly Mesenchymal Stromal Cells Isolated From Umbilical Cord," *Frontiers in Molecular Biosciences* 10 (2023): 1273814, https://doi.org/10.3389/fmolb.2023.1273814.

22. S. Smith, K. Goodge, M. Delaney, A. Struzyk, N. Tansey, and M. Frey, "A Comprehensive Review of the Covalent Immobilization of Biomolecules Onto Electrospun Nanofibers," *Nanomaterials* 10 (2020): 2142, https://doi.org/10.3390/nano10112142.

23. K. A. Callaway, Y. Xue, V. Altimari, G. Jiang, and X. Hu, "Comparative Investigation of Thermal and Structural Behavior in Renewably Sourced Composite Films of Even-Even Nylons (610 and 1010) With Silk Fibroin," *Polymers* 10 (2018): 1029, https://doi.org/10.3390/polym10091029.

24. P. P. Meleiro and C. García-Ruiz, "Spectroscopic Techniques for the Forensic Analysis of Textile Fibers," *Applied Spectroscopy Reviews* 51 (2016): 278–301, https://doi.org/10.1080/05704928.2015.1132720.

25. S.-W. Kuo, "Hydrogen-Bonding in Polymer Blends," *Journal of Polymer Research* 15 (2008): 459–486, https://doi.org/10.1007/s10965-008-9192-4.

26. P. C. Weber, D. H. Ohlendorf, J. J. Wendoloski, and F. R. Salemme, "Structural Origins of High-Affinity Biotin Binding to Streptavidin," *Science* 243 (1989): 85–88, https://doi.org/10.1126/science.2911722.

27. VanadisTM NIPT System, Revvity, accessed January 16, 2026, https://www.revvity.com/category/vanadis-nipt-system.

28. Prenatalsafe®, O., accessed January 16, 2026, https://www.orizzontenascita.it/prenatalsafe/.

29. S. S. Jayashankar, M. L. Nasaruddin, M. F. Hassan, et al., "Non-Invasive Prenatal Testing (NIPT): Reliability, Challenges, and Future Directions," *Diagnostics* 13 (2023): 2570, https://doi.org/10.3390/diagnostics13152570.

30. J.-W. Wang, Y.-N. Lyu, B. Qiao, et al., "Cell-Free Fetal DNA Testing and Its Correlation With Prenatal Indications," *BMC Pregnancy and Childbirth* 21 (2021): 585, https://doi.org/10.1186/s12884-021-04044-5.

31. Rarecells®, R., accessed January 16, 2026, https://www.rarecells.com/brochures.

32. ScreenCell®, S. C., accessed January 16, 2026, https://www.screencell.com/.

33. Parsortix® technology, CelLBxHealth, accessed January 16, 2026, https://cellbxhealth.com/parsortix-technology/.

34. M. Di Trapani, N. Manaresi, and G. Medoro, "DEPArray™ System: An Automatic Image-based Sorter for Isolation of Pure Circulating Tumor Cells," *Cytometry Part A* 93 (2018): 1260–1266, https://doi.org/10.1002/cyto.a.23687.

35. RareCyte®, R. C., accessed January 16, 2026, https://rarecyte.com.